Analysis of the mechanical behaviour of woven fibrous material using virtual tests at the unit cell level

Philippe Boisse, Alain Gasser, Benjamin Hagege, Jean-Louis Billoët

Analysis of the mechanical behavior of woven fibrous material using virtual tests at the unit cell level

PHILIPPE BOISSE
Laboratoire de Mécanique des Contacts et des Solides UMR CNRS 5514, INSA de Lyon, Bâtiment Jacquard, Rue Jean Capelle, 69621 Villeurbanne Cedex, France
E-mail: Philippe.Boisse@insa-lyon.fr

ALAIN GASSER, BENJAMIN HAGEGE, JEAN-LOUIS BILLOET
Laboratoire de Mécanique de Systèmes et des Procédés, UMR CNRS 8106, ENSAM-Université d'Orléans, 8 rue Léonard de Vinci, 45072, Orléans Cedex, France

The determination of the mechanical properties of fabrics in biaxial tension and in-plane shearing is made from 3D finite element analyses of the unit woven cell. Compared to experimental tests these virtual tests have several advantages. They can easily be carried out for sets of varied parameters, they provide local information inside the woven material and above all they can be performed on woven materials that have not yet been manufactured. The 3D computations are not classical analyses because the yarns are made up of several thousands of fibres and their mechanical behaviour is very special. Several specific aspects of the analysis are detailed, especially the use of a hypoelastic law based on an objective derivative using the rotation of the fibre which allows a strict evolution of the directions of orthotropy according to the fibre direction. Examples of analyses are presented in biaxial tension and in-plane shear for woven reinforcements and in the case of the biaxial tension of a knitted fabric. The results obtained are in good agreement with experimental results.

1. Introduction

The development of finite element codes for the simulation of textile composite forming or textile draping [1–3] requires the knowledge and modelling of the mechanical behaviour of woven reinforcements. These are highly specific because of the internal structure of the fabrics (see Section 2). The mechanical behaviour can be investigated by experimental tests such as biaxial tensile tests and in-plane shear tests [4–7].

Section 3 briefly presents two of these tests that will be used for further validations. However, these experimental tests are rather difficult to perform and above all it is sometimes necessary to obtain information on the mechanical behaviour of a fabric which has not yet been manufactured. For instance it may be interesting to know the influence of certain fabric parameters (yarn geometry, yarn density, fibre material, type of weaving. . .) on a forming process. To this end, virtual tests permit the mechanical properties of a woven reinforcement to be obtained relatively easily, without performing the experiments and hence without necessarily manufacturing the fabric under consideration. The virtual tests that are presented in this paper are 3D finite element simulations performed on a unit woven cell. Because of the specific mechanical behaviour of woven material (Section 2), tensile biaxial tests and in-plane shear tests are performed. The finite element of the unit woven cell must account for the constitution of the yarn that is made of thousands of fibres. The specificities of the numerical models will be presented in Sections 3 and 4. This paper will focus particularly on the transverse compaction behaviour and on a hypoelastic model based on an objective derivative using the fibre rotation. Section 5 presents the results obtained in the case of biaxial tension of an unbalanced fabric. Virtual tests in in-plane shear are presented in Section 6. In this case the computation gives correct results but the convergence is not reached after the shear locking angle. Finally a tensile biaxial virtual test on a knitted fabric is presented in Section 7. For all these virtual tests the results are compared to experimental results obtained as described in Section 1. Virtual and experimental tests are in good agreement.

2. Mechanical behaviour specificities of woven materials

The mechanical behaviour of fabrics is complex due to the intricate interactions of the yarns. It is a multi-scale problem. The macroscopic behaviour is highly dependent on the interactions of yarns at the meso-scale (i.e. the woven unit cell) and at the micro-scale (i.e.the fibres constituting yarns). Despite extensive research in the field, there is no widely accepted model that describes accurately all the main aspects of fabric mechanical behaviour. The different model families differ by the scale at which they are defined. A first family of models is obtained by homogenizing the mechanical behaviour of the underlying meso-structure and considering the fabric as an anisotropic continuum [8–10]. While these models can easily be integrated in F.E. classical shell or membrane elements in order to simulate fabric forming, the identification of homogenized material parameters is very difficult, especially because these parameters change when the fabric is strained and when, consequently, the directions of the yarns change. Currently, the continuum models proposed in the literature do not generally account for the interactions between warp and weft yarns (crimp change, locking. . ...). Other authors, in contrast, present fully discrete models of fabrics. Each yarn is modelled and is assumed to be a straight or a curved beam or truss. Springs are usually used to model warp and weft yarn interactions. Many models have been proposed to describe in this way the mechanical behaviour of the unit woven cell submitted to in-plane tension and shear [11, 12]. Some models are extended to the whole woven structure [13, 14]. However, the large number of woven cells in a woven structure leads to high computational cost. We consider a fabric made of two directions (warp and weft) of woven yarns (the classical case) and yarns that are made of juxtaposed fibres (the case for most fabrics used as composite reinforcements) (Fig. 1). All the stiffnesses of a single fibre are very small except for the tensile rigidity in the fibre direction. This is also the case for a yarn because fibres can relatively slide. Consequently the Cauchy stress tensor in the yarn can be assumed to be in the form:

$$\boldsymbol{\sigma} = \sigma^{11}\mathbf{h}_1 \otimes \mathbf{h}_1 \tag{1}$$

where $\mathbf{h}_1$ is the unit vector tangent to the yarn. If a woven domain is considered (Fig. 1b), the stress tensor is in the form:

$$\boldsymbol{\sigma} = \sigma^{11}\mathbf{h}_1 \otimes \mathbf{h}_1 + \sigma^{22}\mathbf{h}_2 \otimes \mathbf{h}_2 \tag{2}$$

where $\mathbf{h}_1$ and $\mathbf{h}_2$ are the vectors in warp and weft directions. The tensions are defined from these stresses:

$$\mathrm{T}^{11} = \int_A \sigma^{11}\mathrm{d}S \qquad \mathrm{T}^{22} = \int_A \sigma^{22}\mathrm{d}S \tag{3}$$

A is the section of the yarn. The tension tensor is limited to:

An in-plane shear rigidity of the fabric is due to the weaving of warp and weft yarns. For a warp-weft angle variation, it can be assumed that a couple C, normal to the fabric, is applied on each crossover, or set of crossovers in the case of more complex woven unit cells. If all the other stiffnesses are neglected, a simplified equilibrium equation can be written for a textile structure with ncell woven unit cells:

$$\sum_{p=1}^{\mathrm{ncell}} {}^{p}\varepsilon_{11}(\boldsymbol{\eta})\,{}^{P}\mathrm{T}^{11}\mathrm{L}_1 + {}^{p}\varepsilon_{22}(\boldsymbol{\eta})\,{}^{P}\mathrm{T}^{22}\mathrm{L}_2 + \sum_{p=1}^{\mathrm{ncell}} {}^{p}C\,{}^{\mathrm{p}}\gamma(\boldsymbol{\eta}) - T_{\mathrm{ext}}(\boldsymbol{\eta}) = 0 \quad \forall \boldsymbol{\eta}/\boldsymbol{\eta} = 0 \text{ on } \Gamma_{\mathrm{u}} \tag{5}$$

ncell is the number of woven unit cells of the textile structure, ${}^{\mathrm{p}}\mathrm{A}$, means that the quantity A is considered for the woven unit cell number p. $T_{\mathrm{ext}}(\boldsymbol{\eta})$ is the virtual work of the exterior prescribed loads. $\varepsilon(\boldsymbol{\eta}) = \nabla^{\mathrm{s}}\boldsymbol{\eta} = \varepsilon_{\alpha\beta}(\boldsymbol{\eta})\mathbf{h}^{\alpha} \otimes \mathbf{h}^{\beta}$ is the symmetrical gradient in the virtual displacement $\boldsymbol{\eta}$ (α and β are indices with the value of 1 or 2). $\mathbf{h}^1$, $\mathbf{h}^2$ are the contravariant vectors related to $\mathbf{h}_1$, $\mathbf{h}_2$ i.e. $\mathbf{h}_{\alpha}$. $\mathbf{h}^{\beta}=\delta_{\alpha}{}^{\beta}$. $\gamma(\boldsymbol{\eta})$ is the virtual relative rotation between warp and weft fibres (or virtual shear angle). L_1 and L_2 are the lengths of the warp and weft yarns in the mid-plane of the fabric. Γ_{u} is the part of the frontier of the domain with prescribed displacements. This equation is much simpler that the general equilibrium equation as it only considers the tensile and in-plane shear strain energy of the fabric. It has been shown on several forming simulation cases that this is sufficient for most of the fabrics used as composite reinforcements [15, 16]. The simplified form of the internal loads virtual power in (5) can be used to build some finite elements made of woven cells in biaxial tension and in-plane shear in order to simulate fabric forming without computing the strain energies that are absent in the case of fabrics [3, 16]. In Equation 5 the mechanical behaviour of the fabric is

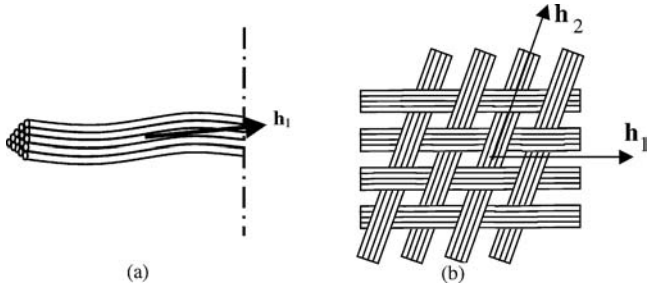

Figure 1 (a) Yarn made of juxtaposed fibres (b) Woven yarns.

determined by T^{11} and T^{22} and C for a given woven cell p. The tensions are function of the strains in both warp and weft directions because of the weaving. Consequently the use of the simplified equilibrium equation requires the knowledge of two tensile biaxial surfaces ($T^{11}(\varepsilon_{11}, \varepsilon_{22})$, $T^{22}(\varepsilon_{11}, \varepsilon_{22})$) and of the shear curve ($C(\gamma)$). The objective of the next sections is the determination of these quantities using virtual and more precisely meso-scale 3D finite element computations of the unit woven cell submitted to biaxial tensions or in-plane shear.

3. Experimental analysis

As seen above, bending and shear stiffnesses are small with respect to the tension stiffness. Therefore, the first point to analyse is tensile behaviour, and, to be more precise, biaxial tension. Indeed, due to the weaving, the change of yarn undulation in one direction has an influence on the other yarn direction. Furthermore, the in plane shear behaviour must be taken into account, since shear is the principal mode of fabric deformation during shaping, and because wrinkling appears when the shear angle exceeds a limit angle (locking angle). The two experiments presented will be important to validate the analyses of the behaviour made using numerical simulations at the unit cell level.

3.1. Biaxial tensile tests

The biaxial tensile device (2a) allows cross specimens to be tested. One of the two deformable lozenges has a modifiable length to obtain different ratios (noted k) between warp and weft strains [7]. Fig. 7 shows the results obtained for different ratios k, for an unbalanced glass plain weave. The curves are different in warp and weft directions because the fabric is unbalanced. The curves exhibit two parts. The first is non linear, due to a change of undulation and/or yarn crushing. The second is linear, and represents the yarn stiffness. The behaviour is the most non linear for a uniaxial tensile test (when a direction stays free of load). With these results, it is possible to build biaxial tensile-strain surfaces [3] which represent the load in a yarn direction versus strain in warp and weft directions. Fig. 2b presents one of these surfaces (in warp direction) in the case of the unbalanced glass plain weave.

3.2. Shear tests

Different in-plane shear tests exist [4–6, 17–20]. In the present study, the tests are performed with a picture frame (3a), made with a deformable frame that prescribes a uniform shear strain field [21]. A camera takes pictures which are processed with a software that gives displacement and strain fields using an image correlation method [22, 23]. Pictures are taken at two scales (macro and meso) to obtain the displacement fields of the whole specimen, but also within a single yarn. The global shear strain field obtained during the deformation is presented in Fig. 4a. The shear curve

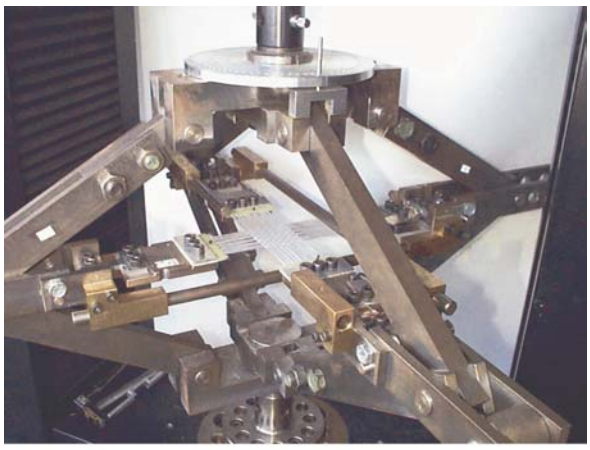

(a)

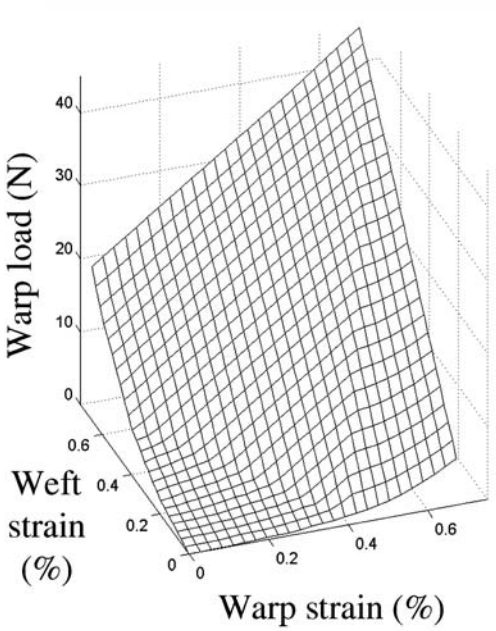

(b)

Figure 2 (a) biaxial tensile device, (b) biaxial tensile-strain surface in warp direction of an unbalanced glass plain weave.

(shear force versus shear angle), presented in Fig. 3b in the case of a glass plain weave, shows three parts. In the first part (up to 35°), the shear force is very small. It corresponds only to yarn rigid rotation as shown in Fig. 4b by the optical method, without yarn deformation: the shear force is due only to friction at crossovers. In the second part, the force begins to increase. Some yarns are in contact with their neighbours and are laterally compressed (see Fig. 4c). In the third part, all the yarns are in contact and compressed (see Fig. 4d) which leads to a marked load increase and to fabric wrinkling. The locking angle (that must not be exceeded to avoid wrinkling) is given by the transition between zones two and three.

4. 3D finite element analyses of the woven unit cell

4.1. Specificities of the analysis

The fabric mechanical behaviour can also be obtained using biaxial tension and shear simulation tests. These virtual tests, i.e. 3D finite elements analyses of a unit

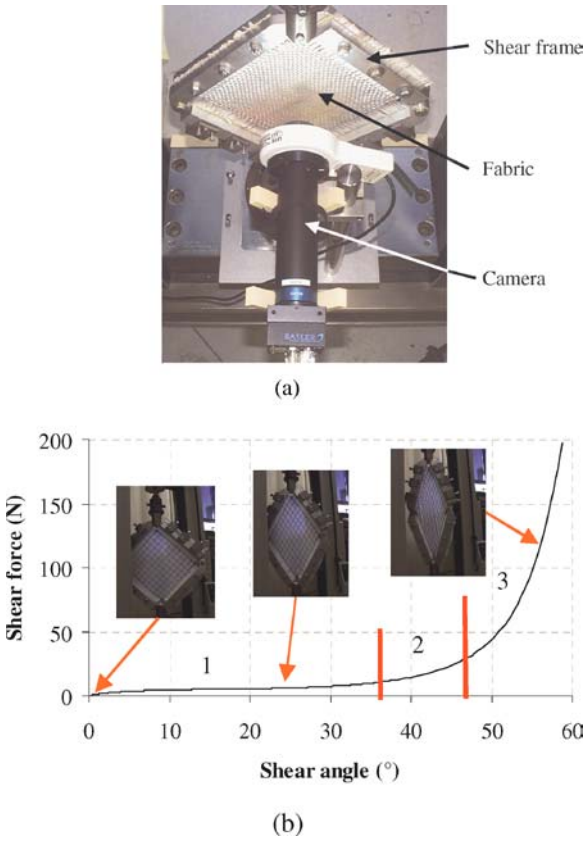

Figure 3 Shear test: (a) picture frame and camera, (b) experimental shear curve on a glass plain weave.

woven cell (representing the periodicity of the fabric) under loading are an interesting alternative. They allow the simulation of many tests that would be costly and difficult to perform in reality, but above all, these virtual tests may be made before the manufacture of the fabric. They also give local information within the material that is very difficult to obtain experimentally. 3D finite element models of the woven unit cell are defined. Contacts between yarns are modelled using a master/slave technique with Coulomb friction. Fabric periodicities, and possible elementary cell symmetry, are represented by boundary conditions. The main difficulty in the analysis is to represent the yarn behaviour with continuum elements while yarns are made of thousands of fibres that can more or less slide relatively. Therefore, like the fabric, yarns have very small stiffnesses in bending and shear. This particular behaviour can be modelled by an elastic orthotropic material, with small transverse Young's modulus (perpendicular to the fibre direction) and small shear modulus with respect to the longitudinal Young's modulus (fibre direction). Longitudinal Young's modulus is identified using a tension test on a single yarn. Transverse Young's modulus is not a constant: it is small at the beginning, but increases as a function of transverse and longitudinal strains. Indeed, the more the yarn is compressed in transverse direction, and tensed in fibre direction, the higher the modulus. Therefore, the crushing law is chosen as

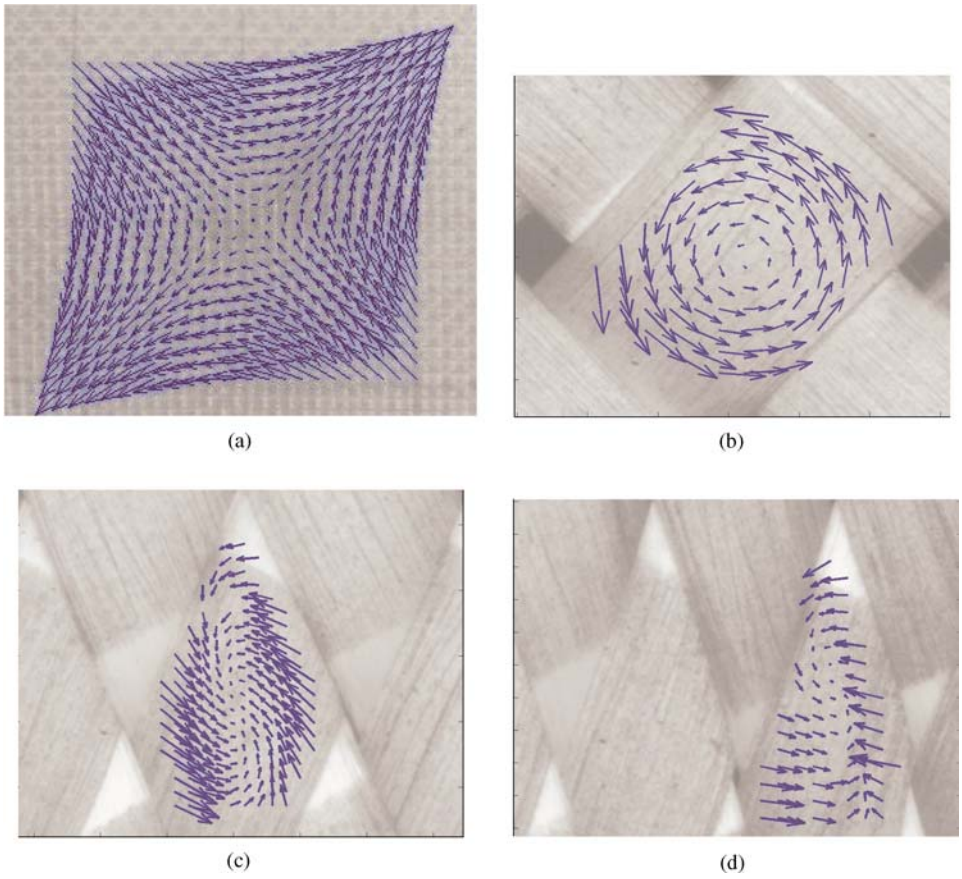

Figure 4 Shear test: Displacement field at macro scale (a), Displacement at meso scale (within the yarn) in zones 1 (b), 2 (c) and 3 (d) of the shear curve (see Fig. 3b).

follows:

$$E_i = E_0 \varepsilon_{11}^m \, |\varepsilon_{ii}|^n + E_\varepsilon \tag{6}$$

where 1 is the fibre direction, 2 and 3 the transverse directions, i is equal to 2 or 3, E_ε is the initial transverse modulus (usually very small), E_0, m and n three material constants. To identify these constants, it is difficult to perform a compression test under different tensions on a single yarn. Hence, they are determined using an equibiaxial tension test on the fabric, coupled with an inverse method [24, 25].

Very weak stiffnesses can lead to numerical problems, such as spurious modes. To avoid these problems, finite elements with reduced integration and hourglass control are used [26]: a stabilization matrix is added to the element stiffness, based on some orthogonality properties of the added fields, to remove the spurious modes.

Since displacements and strains are large, it is necessary to work within a large strain theory. Because Young's moduli are very different in longitudinal and transverse directions, it is important that material directions are followed carefully during analysis. To prescribe these orthotropic axes, the yarn behaviour law is associated with an objective derivative based on the spin of the fibre. This enables the fibre direction to be strictly followed, unlike approaches classically developed in the finite element codes.

4.2. Definition of an equivalent continuum model for fibrous materials

The presented formulation takes the specific mechanical behaviour of fibrous reinforcements into account and is important in 3D finite element analyses of fabric forming. The formulation consists in a hypo-elastic continuous orthotropic model able to cope with large deformations. The specificity lies in the definition of a rotation tensor Δ which we call the "fiber rotation". The latter allows us to model both the evolution of fiber bundles with one strong anisotropic direction and to define a strain measure representative of the transformation of such a medium. This is achieved because Δ enables the fiber direction to be strictly followed, unlike approaches traditionally developed in finite element codes (i.e. Jaumann's corotational formulation [27, 28] or the Green Naghdi approach [28, 29]). When building the FEM, the user has to define the initial orientation of the orthotropic axes along the continuum elements. Generally, these constitutive axes are represented at each Gauss point with the aid of several orthonormal bases κ^0 defined by a rotation tensor field $\mathbf{O}$ that transforms the unitary vectors of the global basis $\{\mathrm{G}\}$:

$$\underline{\kappa}_i^0 = \underline{\underline{O}} \cdot \underline{G}_i \tag{7}$$

The material rotation Δ is then used to update the initial constitutive axes $\{\kappa^0\}$ to the current constitutive axes $\{\kappa^{\mathrm{t}}\}$ (see Fig. 5):

$$\underline{\kappa}_i^t = \underline{\underline{\Delta}} \cdot \underline{\kappa}_i^0 \tag{8}$$

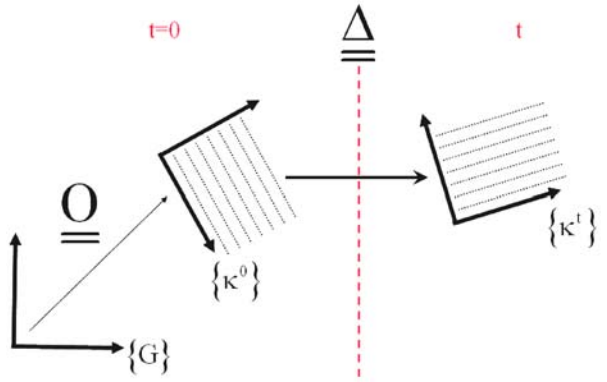

Figure 5 2D representation of the definition of the constitutive axes $\{\kappa^{\mathrm{t}}\}$.

Some developments of Equation 8 ([30]) lead to the set of formula (9) that explicitly give the constitutive axes $\{\kappa^{\mathrm{t}}\}$ as functions of the initial constitutive axes $\{\kappa^0\}$ and the deformation gradient $\mathbf{F}$:

$$\underline{\kappa}_1^t = \frac{\underline{\underline{F}} \cdot \underline{\kappa}_1^0}{\left\| \underline{\underline{F}} \cdot \underline{\kappa}_1^0 \right\|} \qquad \underline{\kappa}_2^t = \underline{\kappa}_2^0 - \frac{b_2}{1+b_1}\left(\underline{\kappa}_1^0 + \underline{\kappa}_1^t\right)$$
$$\underline{\kappa}_3^t = \underline{\kappa}_3^0 - \frac{b_3}{1+b_1}\left(\underline{\kappa}_1^0 + \underline{\kappa}_1^t\right) \tag{9}$$

with $b_k = \underline{\kappa}_1^t \cdot \underline{\kappa}_k^0$ and $b_k \neq 1$. Note that in this formulation the fiber direction, i.e. the strong anisotropic direction, remains aligned with the first vector of $\{\kappa^{\mathrm{t}}\}$. The constitutive behaviour is then fully defined at each time. In fact, the projection (10) of the initial constitutive tensor ${}^0\mathbf{C}$ has known components that can be computed with the traditional engineer's constants ([31]):

$$\underline{\underline{\underline{\underline{{}^0\mathbf{C}}}}} = {}^0C_{ijkl}\underline{\kappa}_i^0 \otimes \underline{\kappa}_j^0 \otimes \underline{\kappa}_k^0 \otimes \underline{\kappa}_l^0 \tag{10}$$

In addition, because the current constitutive tensor $\mathbf{C}$ is supposed to be an objective tensor, it can be deduced from ${}^0\mathbf{C}$ by a rotational transport based on the fourth order rotation tensor $\mathbf{R}$:

$$\underline{\underline{\underline{\underline{\mathbf{C}}}}} = \underline{\underline{\underline{\underline{\mathbf{R}}}}} : \underline{\underline{\underline{\underline{{}^0\mathbf{C}}}}} : \underline{\underline{\underline{\underline{\mathbf{R}}}}}^T \tag{11}$$

In Equation 11, the components of $\mathbf{R}$ are computed from the components of the second order rotation tensor Δ:

$$R_{ijkl} = \Delta_{ik}\Delta_{jl} \tag{12}$$

Lastly, the definition (10) combined with the evolution law (11) entails that the projection (13) of $\mathbf{C}$ is fully known:

$$\underline{\underline{\underline{\underline{\mathbf{C}}}}} = {}^0C_{ijkl}\underline{\kappa}_i^t \otimes \underline{\kappa}_j^t \otimes \underline{\kappa}_k^t \otimes \underline{\kappa}_l^t \tag{13}$$

Thus, the constitutive tensor **C** can be used in a hypoelastic law written:

$$\underline{\underline{L_{\perp/\underline{\underline{\Delta}}}(\underline{\underline{\sigma}})}} = \underline{\underline{\underline{\underline{\mathbf{C}}}}} : \underline{\underline{D}} \tag{14}$$

In Equation 14, **D** is the strain rate tensor and the left member is the Lie derivative of the Cauchy stress tensor with respect to the rotational flow Δ. The geometric definition of this derivative is given by:

$$\underline{\underline{L_{\perp/\underline{\underline{\Delta}}}(\underline{\underline{\sigma}})}} = \underline{\underline{\Delta}} \cdot \frac{d}{dt}(\underline{\underline{\Delta}}^T \cdot \underline{\underline{\sigma}} \cdot \underline{\underline{\Delta}}) \cdot \underline{\underline{\Delta}}^T \tag{15}$$

The cumulated tensorial strain tensor ε and stress tensor σ associated with such an objective derivative are given by:

$$\underline{\underline{\varepsilon}} = \underline{\underline{\Delta}} \cdot \left(\int_0^t \underline{\underline{\Delta}}^T \cdot \underline{\underline{D}} \cdot \underline{\underline{\Delta}} \mathrm{dt} \right) \cdot \underline{\underline{\Delta}}^T \tag{16}$$

$$\underline{\underline{\sigma}} = \underline{\underline{\Delta}} \cdot \left(\int_0^t \underline{\underline{\Delta}}^T \cdot \left(\underline{\underline{\underline{\underline{\mathbf{C}}}}} : \underline{\underline{D}} \right) \cdot \underline{\underline{\Delta}} \mathrm{dt} \right) \cdot \underline{\underline{\Delta}}^T \tag{17}$$

It can be shown that Equation 16 will always give a logarithmic strain in the strong anisotropic direction and that Equation 17 ensures the summation of the stress increments along this direction.

Finally, the use of the material rotation tensor Δ for the Lie derivative (15) and the evolution law (11) entails a consistent approach for fibrous media with one strong anisotropic direction.

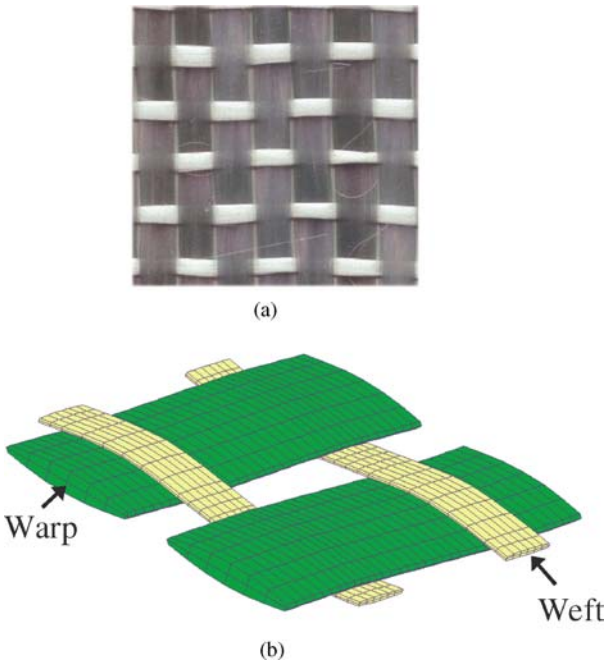

Figure 6 Mesh of the elementary cell (b) of an unbalanced glass plain weave (a).

5. Simulations of a woven unit cell under a biaxial tension

Several elementary cells of different fabrics were analysed for different warp weft strain ratios k. The studied unbalanced glass plain weave is presented Fig. 6a. Elementary cell is shown in Fig. 6b. Due to symmetry, only one quarter is analysed. In the case of equibiaxial load, the obtained transverse strains are large (see Fig. 7a). In the case where one direction is free (uniaxial tension test), it can be seen that the principal mode of deformation is the change of yarn undulation (with small transverse strains). The curves load versus strain for different strain ratios k obtained by the simulations are shown in Fig. 7b and c and compared to experimental results. A good correlation is found. Curves are different in warp and weft directions since fabric is unbalanced. It can be observed on Fig. 7c that the small yarn (weft) has little influence on the great yarn (warp). These analyses (and all those of fabric used for composite materials [3]) show that there is a high degree of crushing and that it is a main aspect of fabric biaxial tension.

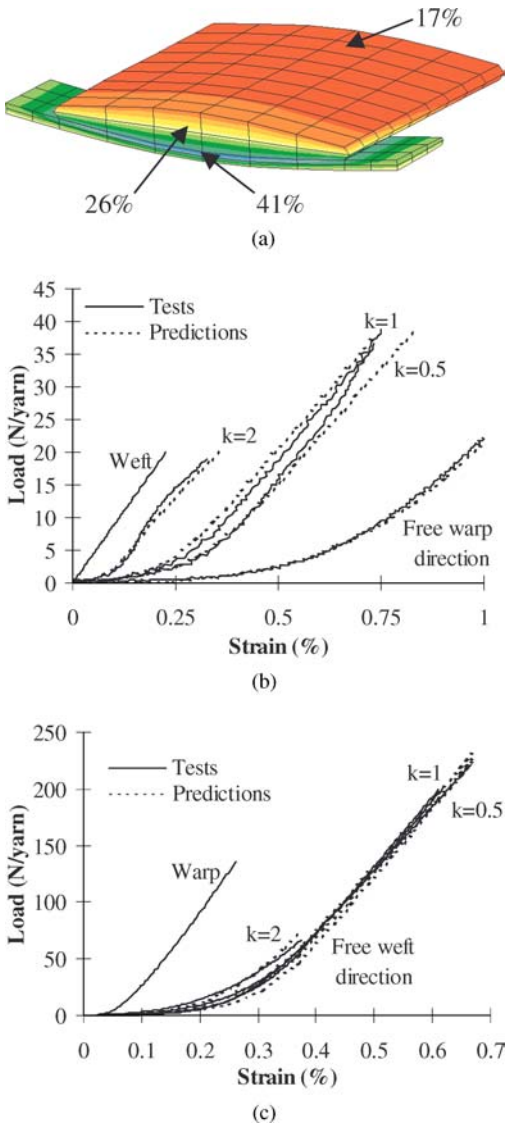

Figure 7 Biaxial tensile simulation on an unbalanced glass plain weave: transverse logarithmic strain for an equibiaxial load (a), experimental/prediction comparisons in weft (b) and warp (c) directions for different values of strain ratio k.

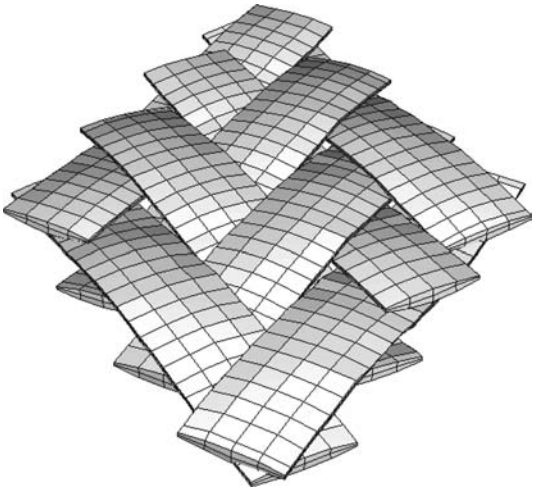

Figure 8 Shear simulation of carbon 2 × 2 twill elementary cell.

6. Simulations of a woven unit cell under in-plane shear

To impose a pure shear on an elementary cell, the kinematics of the picture frame is prescribed as boundary conditions. Furthermore, it was shown experimentally that fabric shear corresponds to yarn rotation without yarn shear (see Section 3.2). Therefore, the yarn sections must stay perpendicular to the middle line. This condition is prescribed to the model.

The finite element analyses are performed using an implicit approach. The results are presented in Fig. 8 for a carbon 2×2 twill, and in Fig. 9 for glass plain weave. The predicted shear curve (Fig. 9) is close to the experimental curve, but the analysis presents a problem of convergence after 45° due to a problem of contact management. It is probably possible to improve this maximum value by using a finer mesh or by performing the analysis with an explicit approach. But the implicit analysis is sufficient to determine the locking angle which is the angle that must not be exceeded during forming if wrinkles are to be avoided.

7. Simulation of the biaxial tension test on a knitted structure

Because of the generality of the formulation described in Section 4.2, knitted structures can also be analysed in case of a biaxial deformation mode. The presented simulation is performed for a biaxial ratio

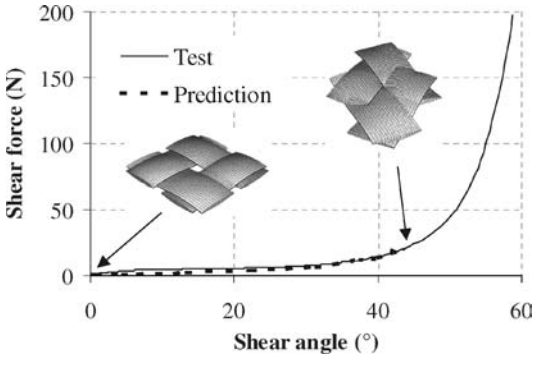

Figure 9 Test/prediction comparison for in plane shear load on glass plain weave.

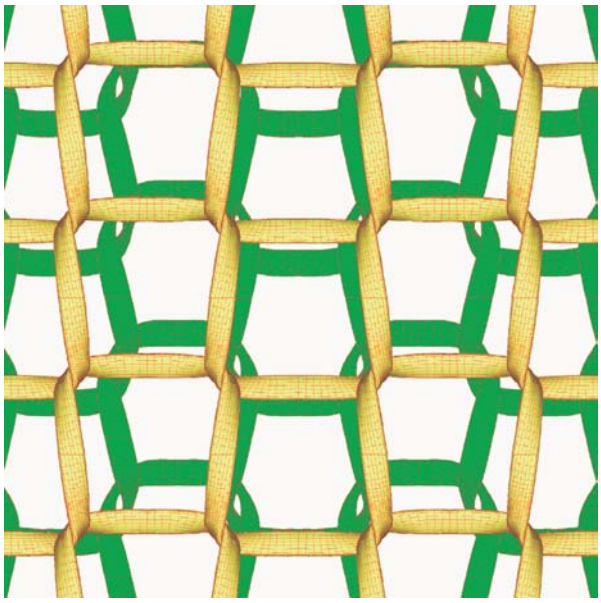

Figure 10 Biaxial test on a knitted reinforcement (Deformed and undeformed virtual samples).

k=1 and the FEM is solved using an explicit code (Abaqus/Explicit). The user routines of this code have permit to implement the approach described in Section 4.2. The studied knitted material is made with aramid yarns and is used as reinforcement in rubber tubes (automotive applications). The deformed virtual sample is very realistic (see Fig. 10) and the load-displacement curves in the directions of loading fit the experimental data obtained from the biaxial tensile test presented in Section 3 (see Fig. 11).

8. Conclusion

The determination of woven fabric mechanical characteristics by mesoscopic 3D finite element analyses of the unit woven cell is an alternative to experimental tests. These 3D simulations present several advantages

- It is easy to vary some parameters of the analysis such as the loading as well as the material characteristics (yarn geometry, yarn density, fibre material, type of weaving...).
- They avoid carrying out experimental tests which can be tricky to perform.
- They give information on the local deformation mechanism within the fabric.
- They can be performed on a fabric that has not yet been manufactured, especially in order to determine its optimal parameters for a given use.

The main difficulty with these simulations lies in the fibrous nature of the yarns that are made of thousand of fibres and the mechanical behaviour of which is very different from a glass or carbon continuous domain. It has been shown that the use of a hypoelasic law based on an objective derivative using the fibre rotation permits to strictly keep the orthotropy directions coinciding with fibre directions. The transverse behaviour law is also an important point since the mesh crushing in a biaxial tension is very large (often larger than

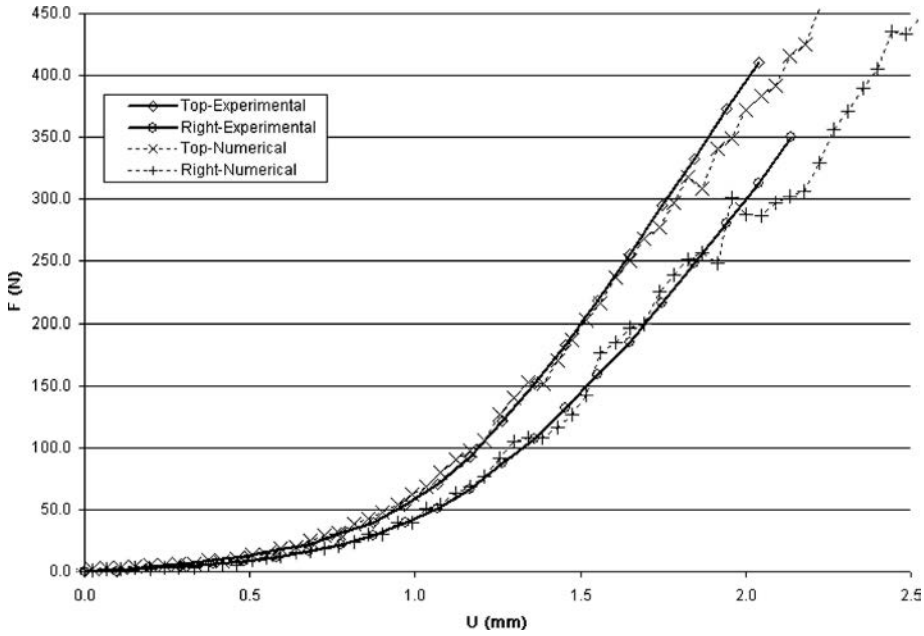

Figure 11 Experimental and numerical load-displacement curves for a biaxial test on a knitted fabric.

40%). The transverse compression law that is used in the present work relates the transverse Young modulus both to transverse strain and strain in the fibre direction. Complementary studies and especially experimental ones will have to be performed in order to define more physically based models and take them into account in the simulations [32, 33].

The presented simulation of the in-plane shear test does not converge when the shear locking angle is exceeded. This difficultly mainly comes from the very complex shape and of the highly localized nature of the contact zone between warp and weft yarns. Work is in progress to overcome this difficulty. In particular, analyses are performed including a local remeshing which considerably increases the number of elements in the contact zone of the warp and weft yarns.

References

1. P. DE LUCA, P. LEFEBURE and A. K. PICKETT, *Composites: Part A* **29** (1998) 101.
2. S.-W. HSIAO and N. KIKUCHI, *Comput. Meth. Appl. Mech. Engng.* **177** (1999) 1.
3. P. BOISSE, A. GASSER and G. HIVET, *Composites Part A* **32** (2001) 1395.
4. A. G. PRODROMOU and J. CHEN, *Ibid.* **28** (1997) 491.
5. T. M. MCBRIDE and J. CHEN, *Compos. Sci. Technol.* **57** (1997) 345.
6. G. B. MCGUINNESS and C. M. O. O'BRADAIGH, *Composites Part A* **29**(1–2) (1998) 115.
7. K. BUET-GAUTIER and P. BOISSE, *Experiment. Mech.* **41** (2001) 260.
8. T. G. ROGERS, *Composites* **20** (1989) 21.
9. A. J. M. SPENCER, *Composites Part A* **31** (2000) 1311.
10. P. XUE, X. PENG and J. CAO, *Ibid.*, **34** (2003) 183.
11. S. KAWABATA, M. NIWA and H. KAWAI, *J. Textile. Inst.*. **64** (1973) 21.
12. T. V. SAGAR, P. POTLURI P. and J. W. S. HEARLE, *Comput. Mater. Sci.* **28** (2003) 49.
13. B. BEN BOUBAKER, B. HAUSSY and J. F. GANGHOFFER, *Comptes-rendus à l'Académie des Sciences de Paris, Série Mécanique* **330** (2002) 871.
14. B. BEN BOUBAKER, B. HAUSSY and J. F. GANGHOFFER, *Finite Element European Revue*, to appear
15. J. L. DANIEL, D. SOULAT and P. BOISSE, Proceedings of the Seventh International ESAFORM conference on Material Forming, Trondheim (Norway), (2004) 301.
16. P. BOISSE, B. ZOUARI and A. GASSER, *Compos. Sci. Technol.* **65** (2005) 429.
17. J. PAGE and J. WANG, *ibid.* **60** (2000) 977.
18. U. MOHAMMED, C. LEKAKOU, L. DONG and M. BADER, *Composites Part A* **31** (2000) 299.
19. M. NGUYEN, I. HERSZBERG and R. PATON, *Compos. Structur.r* **47** (1999) 767.
20. P. HARRISON, M. J. CLIFFORD, A. C. LONG, *Compos. Sci. Technol.* **64** (2003) 1453.
21. A. C. LONG, *Int. J. Forming Process.* **4**(3–4) (2002) 285.
22. P. VACHER, S. DUMOULIN and R. ARRIEUX, *ibid.* **2**(3–4) (1999) 395.
23. F. DUMONT, G. HIVET, R. ROTINAT, J. LAUNAY, P. BOISSE and P. VACHER, *Mécanique et Industries* **4** (2003) 627.
24. D. S. SCHNUR and N. ZABARAS, *Int. J Numer. Meth Engng.* **33** (1992) 2039.
25. A. GASSER, P. BOISSE and S. HANKLAR, *Comput. Mater. Sci.* **17** (2000) 7.
26. D. P. FLANAGAN and T. BELYTSCHKO, *Int. J Numer. Meth. Engng.* **17** (1981) 679.
27. Y. F. DAFALIAS, *Trans. ASME, J. Ap. Mech.* **50** (1983) 561.
28. P. GILORMINI, P. ROUDIER and P. ROUGEE, *Comptes-rendus à l'Académie des Sciences de Paris* **316**(II), (1993) 1659.
29. J. K. DIENES, *Acta Mechanica* **32** (1979) 217.
30. M. A. CRISFIELD, "Non Linear Finite Element Analysis of Solids and Structures, Volume II: Advanced Topics" (John Wiley & Sons, England, 1991).
31. R. JONES, "Mechanics of Composite Materials" (Taylor and Francis, London, 1998).
32. T. G. GUTOWSKI, *SAMPE Quart.* **16**(4) (1985), 58.
33. C. BAOXING and T. W. CHOU, *Compos. Sci. Technol.* **59** (1999), 1519.